Supporting Material for

Measuring molecular motor forces *in vivo*: implications for tug-of-war models of bidirectional transport

Leidel, C.[1], Longoria, R. A.[1], Marquez Gutierrez, F.[1] and Shubeita, G.T.[1,2]

[1] *Center for Nonlinear Dynamics and Department of Physics, The University of Texas at Austin, Austin TX 78712*

[2] *Institute for Cellular and Molecular Biology, The University of Texas at Austin, Austin, TX 78712*

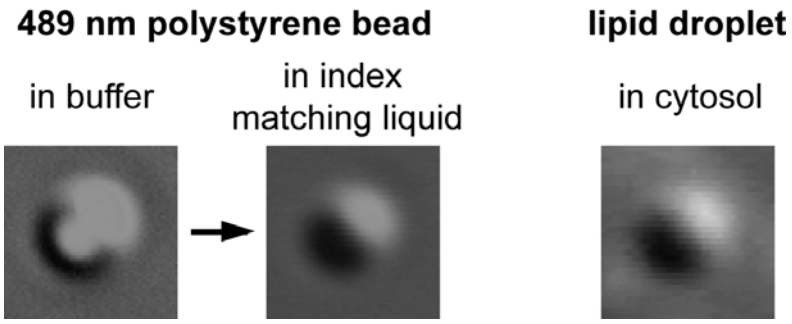

Figure S1 The DIC image contrast arises from the change in the optical path length between the object and the surrounding medium. A polystyrene bead looks like a lipid droplet in cytosol when immersed in an index liquid that matches the index difference; it appears larger and has a different contrast when imaged in buffer. Further, a lipid droplet of the same size as a polystyrene bead will have the same apparent size in the DIC image. As a control, we imaged silica beads (Polysciences) with a mean size of 0.45 μm immersed in water and compared the images to those of 0.45 μm polystyrene beads (Polysciences) in an index matching liquid (aqueous dilution of Cargille index matching liquid). As with the case of lipid droplets, silica beads and polystyrene beads looked similar when index-matched but produced very different DIC images w hen imaged in water (data not shown). The apparent sizes in pixels of both as measured from the cross section was the same, and the difference was smaller than the spread in size of beads of the same material (data not shown).

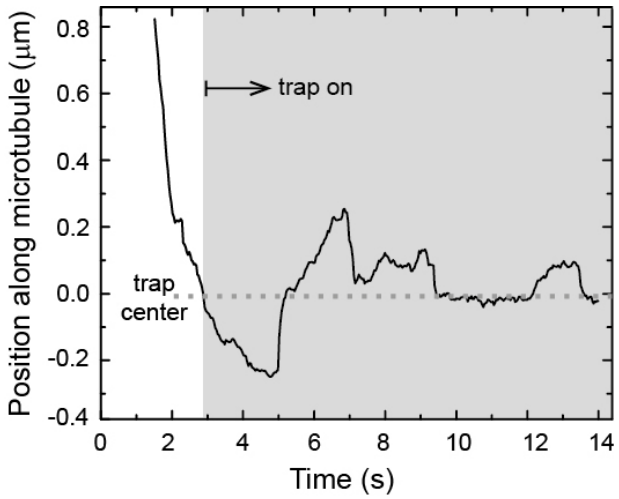

Figure S2: Opposite polarity motors are attached to a single cargo. A trace showing fast direction switching after the minus-end motors detach from the microtubule due to the trap force at ~5.5 s. The plus end motors then pull the lipid droplet in the trap and detach multiple times.

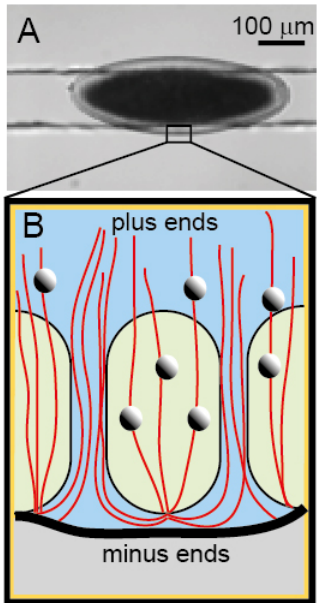

Figure S3: Sample preparation and embryo organization. (A) *Drosophila* embryos were placed in a glass channel and covered by a glass slide for imaging. The area flanking the channel contains nuclei surrounded by the microtubules along which the lipid droplets are transported as schematized in (B). The microtubules (red filaments) are arranged with their minus ends close to the embryo periphery and their plus ends extending inwards. See inset in figure 1A for a high magnification image of the embryo showing lipid droplets.

Supplemental Methods

Real-time particle tracking allowing repeated stall force measurement

For repeated stall force measurements on the same cargo, determining its position as it moves in the field of view is necessary. Since the embryo is thick and full of scattering structures and organelles, the precise and fast quadrant photodiode position detection method could not be used as it utilizes the trap beam emerging from the other side of the sample for position determination (1). Moreover, this method is typically useful to track the position in a maximal range of a few hundreds of nanometers, beyond which it fails. However, cargoes can move more than 10 micrometers along microtubules.

We developed a correlation-based single particle tracking algorithm that can follow the position of the cargo in real-time. Using correlation-based methods the position of the cargo can be determined with a few nanometers of accuracy (2). This made possible multiple stall-force measurements on the same cargo as it moved along its trajectory.

The position of a lipid droplet intended for stall force measurement was tracked in real-time from its DIC video image using a code developed in LabView (National Instruments). The code uses the open CV library (Open Computer Vision version beta 3 available through http://sourceforge.net/projects/opencvlibrary/), as described in more detail in (2), but was optimized for real-time performance (run at 30 frames/s but capable of up to 50 frames/sec).

Sample preparation

Drosophila embryos at the onset of cellularization are dechorionated using fine tweezers and placed at the center of a glass channel surrounded by Halocarbon oil 27 and covered by a cover slide for imaging and optical trapping (Figure S3). Lipid droplets imaged at the edges of the embryos overflowing the channel were well contrasted, and lipid droplets within a few micrometers from the surface were trapped. Embryos continued to develop normally for hours after preparation. The wild type *Drosophila* strain used was YW unless otherwise indicated.

Estimate of the uncertainty in stall force measurements

Given the detailed calibration procedure, an estimate of the uncertainty in the stall force measurements requires considering the different steps involved in the calibration; we estimate an uncertainty of 25% in the individual force measurements as follows. The uncertainty in the lipid droplet size is estimated at 5%. This is mainly due to the finite pixel size as well as the spread in

the data in Figure 1B. This droplet size is used in Figure 1C to get the corresponding stiffness of the trap. Error bars for stiffness in Figure 1C are of the order of 10%. When combined with the uncertainty in the droplet-size determination, this leads to a maximal uncertainty of the order of 15% around 550 nm; the spread of the data around 550 nm leads to a similar estimate of the uncertainty. The stall force is determined by multiplying the stiffness by the measured stall distance from the center of the trap. The latter is subject to noise visible in traces similar to those in Figure 2. An upper bound for this noise is 20%. Combined with the uncertainty in stiffness determination, this leads to an uncertainty in the stall forces reported of the order of 25%.

Determining peak positions in multiple motor force histograms

Determining the peak positions in histograms of stall forces is important to infer biological significance. Given the complexity of the *in vivo* environment, statistics in single molecule measurements could be limited which warrants rigorous statistical analysis to assess the confidence of any conclusions drawn from the histogram. We performed the following tests to determine the best bin size and identify the peak positions for the stall force histogram shown in figure 3 in the main text.

To determine the optimal bin size we used the procedure described in (3). Briefly, the optimum bin size, Δ, is that which minimizes the cost function I -the Mean Integrated Square Error - given by:

$$I(\Delta) = \sum_m \left(A_{m+1} - A_m\right)^2 \times \Delta$$

where A_m is the average of the data in the m^{th} bin. Using this procedure we arrived at the optimal bin size of 0.7 used in figure 3 in the main text. However, it is worth noting that the position of the peaks does not change appreciably (within our uncertainty) for different bin sizes as summarized in the table below.

Bin size (pN)	Position of 1st peak (pN)	Position of 2nd peak (pN)	Position of 3rd peak (pN)
0.53	2.6	5.4	8.7
0.6	2.6	5.5	8.6
0.7	2.6	5.3	8.5
0.8	2.5	5.4	8.3
0.9	2.8	5.6	8.6
1	2.4	5.0	8.1
1.4	2.6	5.5	8.7

Obviously, as one goes to large bin sizes the number of bins becomes smaller and fitting the histogram to three Gaussians becomes meaningless. While the analysis above confirms the robustness of the peak position, it does not rule out the possibility that the measured distribution arises from a single peak (e.g. from one motor exerting a larger force, comparable to that measured *in vitro*). To test this possibility we fitted the relatively smooth histogram of bin size 1.4 pN with a Gaussian distribution. Using χ^2 statistics, we find that we can rule out the null hypothesis that the histogram stems from a Gaussian distribution (p-value = 0.01- 0.04, depending on the number of bins used in the fit).

We used a clustering algorithm to further test whether the data segregate into groups with no imposed functional distribution. As described in (4,5), the optimal clustering found by the algorithm is a tradeoff between a cost function and the quality of the clustering. The quality will obviously be best when each data point is in its own cluster, yet the cost will be high. The cost versus quality relation for the data resulting in figure 3B in the main text is shown below (figure S3), where the number of clusters is labeled for the first few points.

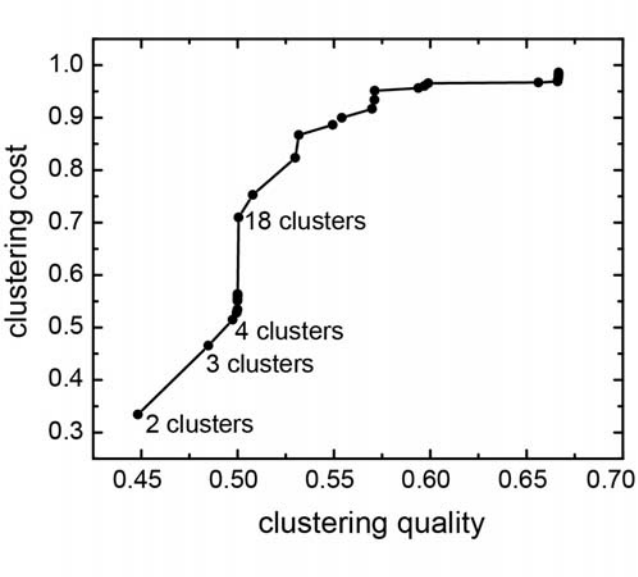

Figure S3: The cost versus clustering quality curve used to find the optimal number of distinct clusters in the data comprising the stall force histogram in Figure 3 in the main text.

The graph shows that the optimal cluster size is four, as going from four clusters to five, six, seven, etc. does not add to the quality of the clustering, but adds cost. However upon examining the four clusters predicted by the algorithm, we find that two of them have means that are indistinguishable given our uncertainty (see table below). Thus, the optimal cluster size is really three. The data that fall in these three clusters (see table below) have averages that agree with the peak positions obtained by fitting the histogram in figure 3 in the main text.

	Average of cluster #1 (pN)	Average of cluster #2 (pN)	Average of cluster #3 (pN)	Average of cluster #4 (pN)
4 clusters	3.1	5.1	6.0	8.5
3 clusters	3.1	5.6	8.5	

Finally, the position of the peaks in the histogram is found to agree (within uncertainty) for two additional sets of measurements using different fly strains, a wild type strain(6) and a mutant in a non-motor protein (Weaver *et al.*, submitted). This analysis confirms that the three peaks in figure 3B indeed represent lipid droplets hauled by one, two and three motors.

Supporting References

1. Neuman, K. C. and S. M. Block. 2004. Optical trapping. Rev Sci Instrum 75:2787-2809.

2. Carter, B. C., G. T. Shubeita, and S. P. Gross. 2005. Tracking single particles: a user-friendly quantitative evaluation. Physical Biology 2:60-72.

3. King, B., M. Stone, H. P. Zhang, T. Gerkema, M. Marder, R. B. Scott, and H. L. Swinney. 2012. Buoyancy frequency profiles and internal semidiurnal tide turning depths in the oceans. Journal of Geophysical Research-Oceans 117.

4. Kannan, R., S. Vempala, and A. Vetta. 2004. On clusterings: Good, bad and spectral. Journal of the Acm 51:497-515.

5. Cheng, D., R. Kannan, S. Vempala, and G. Wang. 2006. A divide-and-merge methodology for clustering. Acm Transactions on Database Systems 31:1499-1525.

6. Shubeita, G. T., S. L. Tran, J. Xu, M. Vershinin, S. Cermelli, S. L. Cotton, M. A. Welte, and S. P. Gross. 2008. Consequences of Motor Copy Number on the Intracellular Transport of Kinesin-1-Driven Lipid Droplets. Cell 135:1098-1107.